# Dynamic behavior of pumps: an efficient approach for fast robust design optimization

**Gabriele Tosi (*), Emiliano Mucchi(*), Roberto d'Ippolito(**), Giorgio Dalpiaz(*)**

(*)Università degli Studi di Ferrara, Engineering Department in Ferrara, Via Saragat, 1 – I – 44122 Ferrara, Italy

(**)NOESIS Solutions, Gaston Geenslaan 11, B4, 3001 Leuven, Belgium

*Corresponding author:*

*Emiliano Mucchi, emiliano.mucchi@unife.it*

*Università degli Studi di Ferrara, Engineering Department in Ferrara, Via Saragat, 1 – I – 44122 Ferrara, Italy*

**Abstract**

Classical design optimization procedures rely on the application of optimization algorithms upon system simulations. These algorithms need a large number of samples to converge on the optimal point. Hence design optimization needs large simulation time since each simulation has to be performed many times. In this paper an original and useful methodology to study and optimize mechanical systems is presented. The proposed methodology combines different techniques such as Design Of Experiments (DOE), Response Surface Models (RSM) and evolutionary algorithms leading to larger time reduction with respect to the classical design optimization approach. On the one hand the proposed methodology gives the optimal combination of variables and on the other hand provides important results to understand the influence of each input to the system outputs. Moreover, a robust design process has been carried out in order to consider the manufacturing tolerances of the real mechanical system and assess their effect on the system performance. The results offer important information and design insights that would be very difficult to obtain without such a procedure. In order to demonstrate the methodology effectiveness, two case studies have been accounted: the optimization of the vibration level of a vane pump and a gear pump. To simulate the dynamical behaviour of the two pumps, mathematical models have been used. These models have been developed and validated by the authors in previous works. The mathematical models include the main important phenomena involved in the pumps operation and they have been validated on the basis of experimental data. The main operational and geometrical input variables have been taken into account in the optimization procedure of such pumps.

Keyword: Optimization; Response surface modelling; DOE; pump dynamics.

## 1. Introduction

Nowadays to remain competitive on the market, many industrial companies focus the attention on the product quality. Consequently there is an increasing interest in studying optimization methodologies applied to simulations in order to find the optimal design performances. The methodology presented in this paper has been developed to help the designer to reach the objective in a reasonable computational time, allowing a “Design Right First Time” approach that leads to shorter time-to-market and reduced costs as compared to conventional “Test, Analyze & Fix”.

This work, intended as an analytical review of the author’s research [1][2][3][4], presents a deterministic and an uncertainty-based analysis. Regarding the first analysis, an optimization methodology has been developed by using mathematical models of mechanical systems in a combined analysis based on Design Of Experiments (DOE) and Response Surface Modelling (RSM). The originality of the proposed methodology consists in the use of DOE, RSM and optimization algorithms for reaching the optimal point, reducing the computational cost with respect to the classical approach used in the optimization process [5] that uses the optimization algorithms directly applied on simulations. Furthermore, such a deterministic study aims at investigating the effect of different pump design variables on dynamic behavior and on pump performance. The uncertainty-based analysis performed in this work takes into account the uncontrollable variations that exist for design variables in reality. It is a robust design analysis performed in order to estimate the sensitivity of output variables to the input uncertainty [6]. From this prospective, one can view robust design as a process of simulation optimization, where the “best” answer is not overly sensitive to small changes in the design input variables.

The classical approach used to find the input configurations that maximize or minimize the objective functions, is to use optimization algorithms directly applied to system simulations. Often these algorithms need many experiments to reach convergence. For this reason in the last years many researchers have worked in the development of new optimization techniques in order to reduce the computational cost or in the development of new efficient optimization algorithms. In particular, in [7] a natural-inspired algorithm called “Teaching–Learning-Based Optimization (TLBO)” has been proposed for the optimization of mechanical design problems; in [8] a method, namely Dynamic-Q, for nonlinear optimizations is discussed. This method needs minimal storage requirements with respect to typical SQP methods, thus making it suitable for problems with a large number of variables. Other works [9][10][11][12][13] focus the attention on the Response Surface Method, exploiting adaptive response surfaces in order to reduce the computational cost for the optimal configuration achievement. In [14], DOE and RSM are used in order to improve an optimization procedure in the thermoscience field; it has to be underlined that in this last research, DOE and RSM are combined in a different way with respect to that proposed hereafter.

In this paper the proposed original methodology has been applied to two different case studies with the main objective to reduce their vibration level. All the optimization steps have been carried out by using Noesis Optimus Rev. 10 as optimization software. The Optimus software has also allowed the automation of the simulation processes and the exploitation of the multiprocessor workstation by the use of parallel computing. The

workstation used to perform all the analyses has Windows 7 Professional as operating system, 12 GB of RAM and twelve processors Intel® Core™ i7 980 @ 3.33 GHz. For both pumps a mathematical model has been built in Matlab/Simulink environment in order to study their dynamic behaviour.

## 2. Optimization Methodology

Generally, optimization strategies rely on specially tailored algorithms for local or global optimizations using simulation codes to assess the objectives that need to be maximized or minimized. The algorithms most frequently used for global optimizations are those of genetic type, which need a high number of simulations to provide sufficient convergence to the objectives, with consequent high computational cost. Following the common optimization strategies, when the algorithm has reached the optimal point, the designer does not have tools for making further evaluations, such as analysis of the solution robustness or assessments on the influence of each input on the component behavior. For these reasons, hereafter a faster methodology is being proposed in order to reduce the overall optimization time and allow the use of efficient global optimization algorithms and meta-modeling techniques. This methodology consists in a combined use of DOE [15][16], RSM [17] and Differential Evolution algorithms [18] for a global optimization [19]. Figure 1 depicts the two common optimization strategies (Methodology A and B) and the novel one (Methodology C). In particular: Methodology A is a combination of mathematical techniques used in the last years for reducing the simulations number in a design optimization; Methodology B depicts the classical optimization method in which optimization algorithms are directly applied on simulations; Methodology C represents the new approach proposed in this article, in which Methodology A and B are combined in order to obtain reliable response surfaces and reliable optimization results with a short number of simulations and an high reduction of computational cost.

The first step of Methodology A (step 1A in Figure 1) is the definition and execution of the DOE. It is well known that DOEs are a systematic approach to get the maximum amount of information out of various types of experiments while minimizing the number of experiments. The second step is the definition of a RSM (steps 2A in Figure 1) based on the experiments performed during the DOE phase. The RSM is a collection of mathematical and statistical techniques useful for the modeling and analysis of problems in which a response of interest is influenced by several variables. The RSM methodology allows DOE results to be exploited in order to build an approximate analytical model of the system response, thus saving the effort of performing additional simulations. Using DOE methods combined with RSM, the response of the system in the points not computed by the DOE can be approximated and predicted efficiently. If a response surface model can be built using DOE results and the quality of the model is sufficient to reliably predict the system response also in other points, then the response surface can become an efficient tool for a fast preliminary optimization. However, the use of response surfaces for optimization has to be done cautiously and ensuring sufficient quality of the response surfaces, that is to say that the response surfaces have to capture the real physics of the system. The quality indexes on the approximation capability of the RSM have been determined by using statistical coefficient $R_{2press}$ [20]. This coefficient indicates the predictive capability of the response surface and reports values between 0 and

1, where values close to *1* (*0*) indicate that the RSM will (not) perform well for points that have not been simulated. Once the quality of the obtained RSM model has been assessed and found to be sufficient, then the optimization algorithm (step 3A in Figure 1) has been performed based on this response surface. The optimal point can be quickly achieved (few seconds) based on such RSM results (step 4A in Figure 1). In order to verify the accuracy of the above-obtained optimal points (step 4A) and in order to assess the effectiveness of this optimization methodology (Methodology A in Figure 1), the optimization algorithm was performed based on simulations rather than on the response surface (step 3B in Figure 1, Methodology B). The problem of the optimization based on simulations is that it could be very time consuming, depending on the complexity of the model to be solved. However, since global optimization algorithms provide optimal results in a region that is very close to the real optimal point, the additional simulation-based local optimization has been performed starting from this first optimal point. In this way, the results of the previous optimization step have been exploited in order to have other simulation results in the zone of interest, i.e. closer to the real optimum point (3B in Figure 1). At the end of the procedure an optimum point can be reached (4B in Figure 1), different with respect to the previous one (4A). In order to refine the solution of this optimum acceleration point, the new simulation results of methodology B and the DOE results of Methodology A have been combined to construct a new response surface (step 2C in Figure 1, Methodology C). It is a response surface of better quality with respect to the response surface estimated on step 2A, since it combines the further simulations performed in step 3B with the simulations performed in the initial DOE (step 1A). This new RSM has also the property of achieving better quality in the region of higher interest, rather than on the whole design domain. Then, a Differential Evolution algorithm can be applied to this new response surface (step 3C) obtaining an optimum point in a few seconds (step 4C in Figure 1). This latter point (4C) is different from the previous ones (4A and 4B), but of improved quality. As a matter of fact, to obtain reliable response surfaces with method A it is necessary a DOE with a larger number of simulations with respect to DOE used in method C. Moreover, in order to obtain reliable results with method B the optimization algorithm requires a larger number of simulations with respect to the algorithm applied to simulations in method C.

The optimization methodology has been fully developed within the Noesis Optimus software. To exploit the full potential of the software in automating the simulations and in the parallel computing, a simple workflowhas been created (see Figure 2). The first workflow block, *Input Variables*, contains all the design input variables with their variability ranges. In the second and third blocks, *Edit Input File* and *Input File*, the values selected by the optimization process are written and stored in an input file. The *Simulation* block reads the input file and then starts and executes the simulation. At the end, the results are saved in an output file (*Output File* block) and are extracted in *Output Variables* block. This workflow has allowed exploiting at the best the twelve processors workstation used for the calculations, carrying out up to ten simulations in parallel with a large saving of computational time. Moreover, the parallel computing has allowed avoiding the interruption of the optimization process due to input configurations that may lead to simulation infinite loops in the calculation (due to possible limitations of the physical model of the two pumps).If one simulation yields an endless loop of calculations, the

parallel computing continues using nine parallel simulations to complete the work. This makes the workflow more reliable.

## 3. Case study 1 – Vane pump optimization

### *a. The mathematical model*

The first case study concerns an oleo-dynamic variable displacement vane pump composed of a cast iron body, in which a one piece rotor shaft, a pressure ring and two port plates are located (see Figure 3). The rotor presents radial grooves in which the vanes can slide. Hereafter, the volume delimited by two consecutive vanes, the pressure ring inner race, the rotor and the port plates is called *vane space*, while the volume defined by the rotor groove, the bottom of a vane and the port plates is defined as *hole*. The port plates present the outlet and inlet ports, suitably designed to communicate both with the vane spaces and the holes. The pump can change its displacement in working conditions to optimize energy consumptions by varying the eccentricity between the rotor shaft and the pressure ring. Thanks to this peculiarity, such a pump can elaborate a “full flow rate” till the desired pressure level is reached, or it can work in a “zero flow condition” maintaining a desired pressure and compensating hydraulic losses. Furthermore, the pump under study can work in a wide pressure range from 20 up to 250 bar. The main operational and geometrical characteristics of the vane pump are listed in Appendix A.

A mathematical model has been developed in order to study the dynamic behavior of the vane pump. This model is a Lumped Parameter (LP) model in which the inertia, the stiffness and the damping properties are taken as lumped. The model takes into account only transversal plane dynamics of the rotor shaft: it is a planar model with 3 degrees of freedom as presented in Figure 4. This model has been developed and validated by the authors in previous works [2][21]. Hereafter only a brief overview is given. The inertia properties of the rotating parts in terms of mass *m* and moment of inertia *J* are considered to be lumped in the rotor portion carrying the vanes (indicated with “*r*” in Figure 4). The degrees of freedom are the displacement along the *x* and *y* directions and angular displacement $\varphi$ of the rotor portion. The known model input is coordinate $\varphi_0$, representing the angular displacement of the rotor shaft section in which the shaft is joined to the electrical motor drive through a key (see Figure 4, shaft portion 1). This shaft section as well as the motor are assumed to rotate at constant speed $\dot{\varphi}_0$ (equal to $\omega$). Coordinate $\varphi_0$ is connected to coordinate $\varphi$ by a torsional spring-damper element that represents the torsional stiffness and the damping of shaft portions 1 and 2 depicted in Figure 4. The shaft torsional stiffness is indicated as $K_T$ and the proportional damping coefficient as $C_T$. The forces and the torques applied to the rotor are pressure forces $F_{rotor,x}$ and $F_{rotor,y}$, journal bearing reactions $F_{b,x}$ and $F_{b,y}$, motor drive torque $M_m$, pressure torque $M_p$, torque due to friction between vane head and pressure ring $M_{vh}$ and torque due to viscous actions $M_{vd}$. The equations of motion, in the reference system depicted in Figure 4, can be written as follows:

$$\begin{cases} 2F_{b,x} + F_{rotor,x} = m\ddot{x} \\ 2F_{b,y} + F_{rotor,y} = m\ddot{y} \\ M_m + M_p + M_{vh} + M_{vd} = J\ddot{\varphi} \end{cases} \quad (1)$$

where *m* is the mass and *J* is the moment of inertia of the rotating parts. In order to solve these equations of motion, the loads involved in terms of pressure forces and torques should be determined. These loads directly depend on the pressure field inside the pump. The variable forces acting on the pump casing are due to variations in the pressure field that has been modeled by means of an Euler's approach, as proposed in [3][21][21][22]. Using this modeling technique, the pump fluid domain is divided into several control volumes; each control volume is treated as an open thermodynamic system with mass transfer with its surroundings. By using the relation presented in Eq. (2), it is possible to determine the pressure variation inside control volume $i$ caused by flow rate gain $\Delta Q_i$ and by the volume variation of $\frac{dV_i}{d\varphi}$. In Eq. (2), $\omega$ is the rotor angular speed, $B_{oil}$ is the isothermal Bulk modulus of the oil, $p_i$ represents the pressure of control volume $i$, $V_i$ is its volume and flow rate gain $\Delta Q_i$ is the balance between the flows coming in and out from control volume *i*:

$$\frac{dp_i}{d\varphi} = \frac{B_{oil}}{V_i\omega}\left(\Delta Q_i - \frac{dV_i}{d\varphi}\omega\right) \quad (2)$$

The pressure field can be finally obtained by integrating the system of flow rate continuity equations. Once the pressure field is determined, it is possible to calculate the main excitation forces that load the pump components. The journal bearing reaction and the forces acting on the pressure ring have been combined with the experimental *frequency response functions* (FRFs) of the pump casing to calculate the casing accelerations that are the main sources of noise and vibrations. These accelerations have been compared with measured accelerations in the validation procedure. Figure 5 depicts the results in terms of pressure evolution for a complete shaft rotation in a vane space and in a hole. The passage from the inlet to the outlet region can be immediately distinguished and the ripple phenomena for the high pressure region are underlined as well. The reference system used to plot the pressure evolution in Figure 5 is depicted in Figure 3: the angular coordinate reference starts from −Y direction. Quantity $p^*$ represents the normalized pressure:

$$p^* = \frac{p}{p_{outled}} \quad (3)$$

where pressure $p_{outled}$ is the constant operational pressure in the outlet chamber. Both the plots depict pump behavior in the full flow rate condition. The pressure evolution are compared and validated with respect to measured data. The simulated pressure shows a good concordance with the measured pressure.

*b. Input – Output variable definition*

Three geometrical inputs and one input relative to oil characteristics have been considered. According to pump design, stepped values in the actual variability range have been selected for all the variables (see Table 1). The ratio between air volume and oil volume in the oil has been chosen to estimate the influence of the percentage of air dissolved in the oil. It is important to underline that a change of this ratio determines a change in the oil Bulk modulus. The geometric inputs concern the clearances between some components. Particularly the radial clearance in the journal bearings, the clearance between the rotor and the port plates and between the pressure ring and the port plates have been considered. It has to be underlined that a variation of the clearance in the journal bearings determines different bearing reactions leading to different shaft accelerations. On the other hand, a variation of the meatus thickness mentioned above (see Table 1) determines different pressures in the vane spaces and holes and therefore different variable pressure forces [23]. The optimization objectives for this pump were the minimization of the vibration level and the maximization of the pump efficiency. The Root Mean Square (RMS) acceleration in four points of the external casing has been considered (Figure 6) based on one acceleration in Y direction (acc_1), two in X direction (acc_2 and acc_4) and one in Z direction (acc_5). The mean volumetric flow rate (Out_flow) has been calculated to estimate the pump efficiency.

*c. Optimization results*

The three methodologies presented in Section 1 have been applied to the vane pump case study in order to assess their effectiveness and efficiency. A DOE has been set up to explore the whole input domain with a limited number of simulations (step 1A of Figure 1). Among different kinds of DOE, the Latin Hypercube Design DOE has been selected due to the specific suitability to build response surfaces and for the uniform coverage of the input design space. For a complete description of Latin-Hypercube Design (LHD) refer to [20]. For the present case, a LHD DOE of 300 experiments has been considered. The DOE construction results the slowest methodology step (step 1A of Figure 1), due to the high number of simulations to be performed. Each vane pump simulation requires about 45 minutes to be executed. Thus, a DOE with 300 experiments would need 10 days to be completed. By exploiting the workflow developed in this work (Figure 2), it was possible to realize parallel computing and perform 10 simulations simultaneously. In this way only one day of computational cost was needed to complete the DOE step. One of the most important results of DOE is the correlation matrix which contains the correlation coefficients for the DOE accounted. The value of this coefficient varies between 1 and -1, where *1* indicates a perfect direct correlation, *-1* a perfect inverse correlation and *0* the absence of correlation.

Figure 7(a) depicts the correlation matrix between the output variables for the vane pump DOE. The accelerations are directly correlated; in particular a strong correlation between the two accelerations in X direction (acc_2 and acc_4) and the acceleration in Z direction (acc_5) occurs. Also acc_1 is directly correlated with the other accelerations. This direct correlation suggests that by minimizing one acceleration also the others should be reduced. Acc_2 has been selected as optimization objective since using input variables with nominal values (Table 1), acc_2 becomes the highest values with respect to the other acceleration points. Moreover all the accelerations have an inverse correlation with the mean output flow rate (Out_flow). Consequently by maximizing the output flow rate, all the accelerations should maintain low values, and vice versa by minimizing the accelerations the flow rate should reach a high value. Therefore, two single-objective optimizations have been considered in the methodology, one to minimize acc_2 and one to maximize Out_flow. Figure 7 (b) shows the correlation coefficients between inputs and outputs. These coefficients emphasize that the ratio between air and oil volume has the highest influence on the output, in particular a strong inverse correlation between this ratio and the mean output flow rate occurs.

On the basis of DOE results, different response surface models have been built with the aim of selecting the combination of input variables (indicators) that predicts the system response at the best. The evaluation of the predictive capability of these indicators (normal regression parameter and adjusted regression parameter, see [20]) and the comparison between simulations and RSM results have allowed the choice of the appropriate surface. The Least-Squares with Taylor cubic polynomial algorithm [20] gives the best response surface and it has been used both for the acceleration and for the mean output flow rate objectives. Statistical coefficient $R^2_{press}$ results equal to 0.5 for acc_2 and 0.97 for Out_flow. Thus the RSM is reliable only for the flow rate, since the predictive quality for acc_2 is not considered sufficient. As a matter of fact there is a small difference (residual) between RSM and simulation results for the flow rate (Figure 8(a)) while for the acceleration the difference is larger (Figure 8(b)). Following Methodology A, two single-objective optimizations have been performed, one to minimize the flow rate and one to maximize the acceleration. The Differential Evolution (DE) algorithm based on RSM has been used for both the optimizations and the optimal configuration was reached in a few seconds. The results obtained are presented in Table 2 and Table 3 (Methodology A). Since the RSM of the acceleration was not reliable, it was necessary to execute other analyses following step 3B of the methodology. Therefore the DE based on simulation has been forced to execute a few simulations to minimize the acceleration. As previously mentioned this step is very useful to increase the number of results in the zone of interest. A DE algorithm with a maximum number of experiments equal to 15 and a population of 10 elements for each iteration has been created. The DE algorithm executed all the 150 experiments in 5 hours of computational cost. The optimal configuration reached in step 3B is presented in Table 3 (Methodology B).

Once completed step 3B, the new simulations results are combined with DOE results. These data are used to build new response surface models (step 2C). The Least-Squares with Taylor cubic polynomials method gives the best RSMs also for step 2C. Statistical coefficient $R^2_{press}$ for these new RSMs is 0.87 for the acceleration and

0.97 for the output flow rate. The comparison between Figure 8 and Figure 9 shows that step 3B has allowed making the new RSM reliable in the zone of interest, i.e. where the acceleration has a low value. In this zone (red oval in Figure 9) a little difference between simulation results and RSM results occurs. Therefore the new RSM can be considered reliable and can be used for optimizations and other evaluations. Figure 10 and Figure 11 present the new response surfaces. Figure 10(a) highlights a strong linear dependence between the mean output flow rate and the ratio between air and oil volume, while the variation of the other inputs does not cause great variation on the output flow rate. Figure 11(a) and (b) depict the response functions for the acceleration. It is worth noting that every input variation causes consistent variation in the acceleration value, but the ratio between air and oil volume is the input that determines the larger output variation as occurs for the Out_flow. Finally two single-objective optimizations have been performed (one to minimize acc_2 and one to maximize Out_flow) using the DE algorithm applied to the new RSM with a maximum number of iterations equal to 70 and a population of 20 elements for each iteration. The two optimizations needed a few seconds to reach the optimal configurations, see Table 2 and Table 3 (Methodology C). Table 2 shows that the two methodologies have reached the same input configuration but with a slight difference in the numerical result. The simulation result corresponding to this input configuration is 0.3909 $m^3/s*10^{-3}$. Thus concerning the Out_flow output, Methodology A gives a numerical error equal to 0.55% while Methodology C gives a numerical error equal to 0.05%. Therefore Methodology C gives more reliable results than Methodology A.

Taking the values collected in Table 3 as a reference, Methodology A gives the lowest value of acceleration. However the simulation result corresponding to this input configuration leads to an acceleration of 227.29 $m/s^2$. Thus, Methodology A cannot be used since the RSM based on DOE is of bad quality. The simulation result with the configuration of Methodology C is 214.22 $m/s^2$. For this reason it is possible to conclude that Methodology C allows to reach the best optimization result.

*d. Robust design analysis*

In the engineering field, the traditional design optimization model generates deterministic optimum designs. However, the existence of uncertainties in physical quantities, such as manufacturing tolerances, requires a robust design approach to design optimization. Uncertainties may lead to variation in the studied system performance. For this reason the optimal performance should be the least sensitive to the variability of the uncertain variables. Robustness analysis aims at estimating the sensitivity of the outputs to the input variability [24]. The robust design approach was pioneered by Genichi Taguchi for quality planning and engineering product design activities. He found that it was often more costly to control causes of manufacturing variations than to make a process insensitive to such variations [25]. In this work the uncertainty of all the input variables has been considered. The uncertainty of the geometrical inputs has been identified as due to the manufacturing tolerances. The uncertainty of the ratio between air and oil volume is due to the fact that it is not possible to know this ratio in operational conditions a priori but only to suppose it. For all the input variables, a normal distribution around the optimum value is considered. The tolerances and standard deviations considered in the robust design analysis are presented in Table 4. In order to assess the effect of input uncertainty on system

responses, an analysis method to propagate uncertainties in the simulation process has been adopted. This method is directly implemented in the simulation workflow of Figure 2. In this way, the quantification of the robustness of the system can be quickly assessed by directly using the same simulation workflow and response models previously created. The robustness of the output results has been quantified by using the standard deviation as the main parameter. In particular, the smaller the standard deviation of the output is, the more robust the output becomes.

Two robust design analyses have been performed, one based on the optimization of the volumetric flow rate and one based on the acceleration optimization. For each analysis, a Monte Carlo method [26][27] combined with the Latin Hypercube sampling has been used, with the aim at obtaining the output standard deviations due to the input variability [28].1500 samples are taken for every Monte Carlo analysis. These samples are obtained from the new RSM and for that reason also this analysis needs only a few seconds to be completed. The outcomes of the Monte Carlo analyses are histograms that represent the probabilistic distribution of the system responses. Figure 12 presents the distribution of the experiments performed during the Monte Carlo analysis. In particular the distribution is calculated both for the volumetric flow rate (Figure 12 (a)) and for the acceleration (Figure 12 (b)). The red bar in the figures represents the optimal points. The standard deviation was about 0.17% for the volumetric flow rate and about 0.91% for the acceleration. It is interesting to note that for both the outputs, the most probable values are very close to the optimal value, yielding a probability distribution close to a normal (or Gaussian) distribution. Furthermore both the standard deviation values are very low. Thus the optimal configurations are not significantly influenced from a little input variability.

## 4. Case study 2 – Gear pump optimization

### *a. The mathematical model*

The second case study addresses an external gear pump for vehicle steering. This pump uses a simple mechanism to produce flows and to increase the fluid pressure. It combines good performance and low cost. In this type of gear pump mainly two sources of noise can be identified, one due to the fluid flows that pass from the low to the high pressure chamber, and one due to the variable meshing stiffness during the gear rotation. Such excitations depend on numerous variables that increase the complexity of the study of the system. The pump has two twin gears of 12 teeth (see Figure 13), which are assembled by a couple of lateral floating bearing blocks that act as seals for the lateral ends. Gears and floating bearing blocks are jointly packed inside a casing that encloses both the components and defines the isolated spaces that carry the fluid from the low to the high pressure chamber. These lateral floating bearing blocks act as supports for the gear shafts by means of two hydrodynamic bearings, which are hydraulically balanced in order to avoid misalignments between gear shaft and journal bearing. In the gear meshing area, when two tooth pairs come into contact, a trapped volume could arise and could undergo a sudden volume reduction and consequently a violent change in its pressure. To avoid this, the trapped volume is put in communication with the high or low pressure chambers. That is the role of the relief grooves milled in the internal face of the bearing blocks whose shape and dimension are very important in

the resulting dynamic behavior. The main operational and geometrical characteristics of the gear pump are listed in Appendix A.

In order to study the pump dynamic behavior during operational conditions, a combined lumped-parameter finite-element (LP-FE) model of the pump is used. This model has been developed and validated by the authors in precedent works [3][4][23][29][30]. In this section the model will be shortly described. The LP model is a planar model with 6 degrees of freedom. For each gear degrees of freedom are the displacements along the directions X and Y in Figure 14 and the angular displacement. The model includes the main important phenomena involved in the pump operation such as time-varying oil pressure distribution on gears, time-varying meshing stiffness and hydrodynamic journal bearing reactions. The LP model takes into account the dynamic behavior of the moving components of the pump and gives as output the dynamic forces and torques acting on gears. In particular, the forces exchanged between the gears and the casing are the pressure forces and bearing reactions. These are the forces exciting the casing vibrations. On the other hand, the FE model considers the external pump casing in order to calculate the acceleration on the external surfaces of the pump. Particularly, the FE model of the pump casing was developed and used in order to estimate the frequency response functions (FRFs); they are the transfer functions between the internal part of the pump, where the exciting forces applied by the gears act, and the external surface of the casing. Finally, the acceleration of the casing surface is evaluated in different operational conditions by multiplying the above-mentioned FRFs by the spectra of the exciting forces estimated with the LP model. In this context, the dynamic model can be considered an effective LP-FE model for the evaluation of the casing vibration due to the dynamic behavior of the pump rotating components. In the LP model, the meshing phenomena have been widely developed. The model takes into account the parametric excitations due to the time-varying meshing stiffness and the tooth profile errors (obtained by a metrological analysis); the effects of backlash between meshing teeth, the lubricant squeeze and the possibility of tooth contact on both lines of action were also included in the model. The oil pressure distribution on gears is also time-varying [31][32]: it is instantaneously computed and the resultant force and torque are obtained taking into account the case wear as well as the displacement of the lateral floating bearing blocks. The non-linear behavior of the hydrodynamic journal bearings is also included [33].The non-linear behavior of this kind of bearing has been modeled using Child's theory called "finite impedance formulation" [33]. In brief, this formulation consists in taking into account and composing the results from "*short bearing*" and "*long bearing*" theories. This formulation leads to obtain the bearing reactions. Such a formulation states that the magnitude of the reaction forces in the journal bearings increases as rotational speed, lubricant oil dynamic viscosity, eccentricity ratio of the journal axis and its derivatives increase and as the ratio between radial clearance and journal radius decreases. Moreover, the torsional stiffness and damping of the driving shaft is considered. As a consequence, the model is highly nonlinear. All these components are included in the equations of motion (Eqs. (4-9)) written in the reference systems of Figure 14 [3][4]:

$$\begin{cases} m_1\ddot{x}_1 = f_{bx1} + f_{px1} \\ m_1\ddot{y}_1 = f_{by1} + f_{py1} + f_{mg} \\ J_1\ddot{\theta}_1 = -r_b f_{mg} - M_{p1} + M_m \\ m_2\ddot{x}_2 = f_{bx2} + f_{px2} \\ m_2\ddot{y}_2 = f_{by2} + f_{py2} - f_{mg} \\ J_2\ddot{\theta}_2 = r_b f_{mg} - M_{p2} \end{cases} \quad (4\text{-}9)$$

These equations give the dynamic equilibrium between the pressure forces and torques ( $f_{pxi}$, $f_{pyi}$, $M_{pi}$ ) acting on the gears, the meshing forces ( $f_{mg}$ ), the driving external torque ( $M_m$ ), the bearing reactions ( $f_{bxi}$ , $f_{byi}$ ) and the gear inertia forces and torques. Note that subscript "i" denotes gears: gear 1 is the driving gear, gear 2 is the driven gear. The solution of (4-9) leads to obtained the translational gear vibration along $X_i$ and $Y_i$ coordinate axes as well as the torsional gear vibration around $\vartheta_i$ coordinates. The vibratory behavior of the gears in the $X_iY_i$ plane can therefore be estimated. The FE model not only regards the pump casing, but also the plate to which the pump is fastened during the experimental tests. In more details, the FE model includes all the non-rotating components of the pump: the casing, the two end-plates (the lower one is indicated as flange and the upper one as cover), the valves, the bearing blocks, the ergal plate to which the pump is fastened on the test bench as well as the four force sensors supporting the plate (more details are given in [4]). The masses of the two gears are not included in the FE model because their inertial contribution is already taken into account by means of the dynamic forces computed by the LP model. The ergal plate is connected to ground by means of four triaxial force sensors located under the ergal plate.

An FRF analysis has been performed on the FE model. It consists in a dynamic analysis in which the input point is located in the gear house (point A in Figure 15): it is the excitation point where the dynamic forces act. The output points (response points) are placed in the two opposite external surfaces of the casing (points B and C in Figure 15). It is worth noting that the damping introduced in the FRF analysis is evaluated by means of an experimental modal analysis. As an example of simulation results Figure 16 depicts the pressure force $f_{px1}$ on gear 1 as a function of the meshing period, with different relief groove dimensions (dimension B in Figure 14). Important variations are due to the phenomena concerning the trapped volume, occurring when its connection with the input volume begins at about 16% of *T*, and when its connection with the output volume ends at about 20% of *T*. Another large variation takes place when the number of the isolated tooth spaces increases from 6 to 7, at about 25% of *T* for gear 1. On the contrary, the force variation is small when the number of the isolated tooth spaces decreases from 7 to 6, that is to say, when an isolated space begins to be opened on the output volume, at about 61% of *T* for gear 1; in this case the force variation is small presumably because, before this space is opened, its pressure is already very close to the output pressure.

*b. Input – Output variable definition*

The following six input design variables are considered in the optimization process concerning acceleration: output pressure, rotational speed, relief groove dimension (dimension B in Figure 14), radial clearance in the journal bearing, oil Bulk modulus and oil dynamic viscosity. The output pressure and the rotational speed have been considered as fix input variables since in standard test conditions such values are always taken constant at 70 bar and 1660 rpm, respectively. The relief groove dimension and the radial clearance have been introduced as stepped values in a range according to pump design. It is worth noting that the step variations reflect values that could be manufacturing in the actual machining process. Two inputs related to the characteristic of the lubricant oil have been chosen: the dynamic viscosity and the Bulk modulus. The viscosity mainly depends on pressure and temperature. In this study, the pressure is taken as constant, therefore only the dependence on temperature is accounted. Regarding the Bulk modulus, it mainly depends on pressure, temperature and air fraction in the oil mixture. Considering what stated above, only the dependences on temperature and air fraction have been accounted. In [23] it has been showed that the Bulk modulus is nearly constant at high pressure (60 to 100 bar) also if the air fraction increases of two magnitude orders. So this latter dependence has been neglected. In this work, the Bulk modulus and the oil viscosity have been considered depending on temperature only, determining these values at the constant pressure of 70 bar. The operational temperature of the pump ranges from 40 to 100 °C that corresponds to a variation of 3003 bar for the Bulk modulus and of 10.11 mPa*s for the dynamic viscosity (see Table 5).Therefore, four different temperatures (40, 50, 80, 100 °C) have been chosen as representative of the oil characteristic that correspond to four precise Bulk modulus and viscosity values. In practice, the analysis aims at studying the behavior of a specific oil as a function of the operational temperature ranging from 40 to 100 °C. A summary of the selected values for every input variable is shown in Table 5. The chosen output variable is the Root Mean Square (RMS) value of the acceleration in the two points of the external casing (points B and C in Figure 15). The two accelerations depend on the same dynamic forces and in principle they are different because different are the FRFs between the input point and the response points. However, in this analysis the two FRFs are similar in the frequency range of interest, due to the pump casing geometry. Therefore, the input configuration that determines the minimum acceleration at point C is the same that determines the minimum acceleration at point B. For this reason, the optimization is carried out considering point C only.

*c. Optimization results*

Considering the low knowledge and the complexity of the solution domain, the DOEs performed in this work (steps 1A in Figure 1) are Latin-Hypercube Designs (LHD) of 45 experiments each. An experiment needs about fifteen minutes to be executed. This means that 11 hours are necessary to complete the DOEs. Taking advantage of the parallel computing, ten simulations contemporaneously can be executed and the DOEs can be completed in one hour and a half. The average correlation coefficients between input and output parameters are computed over the whole explored design space as representative of the principal linear correlation coefficients. These coefficients are presented in the correlation matrix of Figure 17. Some remarks can be drawn. Firstly, the

oil temperature plays a pivotal role with respect to the acceleration, because of the highest absolute correlation value (0.935). Secondly, the other inputs have low correlation values, so their influence on the output is less important. The second step of the methodology (step 2A of Figure 1) consists in the creation of an RSM based on the DOE results. The Least-Squares method with cubic Taylor polynomials [20] has been firstly selected as RSM concerning acceleration. However, this RSM was not satisfactory, as displayed in Figure 18 in which the difference between the RSM and simulation results is evident (10% as average value) and statistical coefficient $R^2_{press}$ is rather low (0.78). So, it was necessary to develop an *ad hoc* response surface by selecting, among a potentional functional basis, the functional that more deeply influence the overall response.

As an example, Figure 19 shows the first six input functionals of the contribution plot concerning the acceleration. They have been used for the definition of the *ad hoc* response surface. In particular, the *ad hoc* response surface has been created by using the 18 most dominant terms of the contribution plot. Particularly, this *ad ho*c response surface for the acceleration is of least-squares type and composed of the following terms : $1,\ T\ ,\ Cr\ ,\ B\ ,\ T^2\ ,\ T^3\ ,\ Cr*T\ ,\ \cos(T)\ ,\ B*T\ ,\ B*Cr*T\ ,\ B*Cr\ ,\ \cos(Cr)\ ,\ \sin(T)\ ,\ B^2\ ,\ Cr^2\ ,\ Cr*T^2\ ,\ Cr^2*T\ ,\ \cos(B)$. The *ad hoc* response surface is of improved quality with respect to the “Taylor polynomials” based being its statistical coefficient $R^2_{press}$ is close to 1 (0.92). Concerning step 2C in Figure 1, the used response surface is a classical “Interpolating-RBF-Cubic” response surface [20] based on DOE and optimization results. Three examples of response surface results are presented in the 3D graphs of Figure 20. They are the *ad hoc* response surfaces obtained in steps 2A. Response surface in Figure 20(a) is obtained at constant relief groove dimension (*B=1.3mm*), response surface in Figure 20(b) is obtained at constant radial clearance ($C_r$=0.026mm) and response surface in Figure 20(c) at constant oil temperature (T=40°C). The surface of Figure 20(a) highlights the strong relation between temperature and acceleration, i.e. the lower the temperature is, the lower the acceleration becomes. The 3D graph of Figure 20(b) presents the response surface of the acceleration as a function of temperature and relief groove dimension: the acceleration decreases with the decrease of the temperature, while the dependence on the relief groove dimension presents a local minimum in the accounted domain. Finally, Figure 20(c) depicts the influence of relief groove dimension and radial clearance on the acceleration. This surface is more complex than the others, since many local minima occurs in the domain takes into account.

Concerning the optimization process, it consists in the calculation of a single-objective optimization with the aim of minimizing the RMS value of the acceleration. The Differential Evolution algorithm has been selected. This algorithm has proved to be the most suitable for complex problems where no a priori assumption can be made on the monotonicity or not of the system responses of interest. This algorithm is known to be more computationally expensive than other evolutionary or genetic algorithms, but its stability properties make it a good reference candidate for the present case. Since the computational effort to run this algorithm on a response surface is negligible, the DE algorithm has been selected for this phase of the optimization. As

discussed in Section 1 and depicted in Figure 1, three different scenarios have been followed in order to obtain the optimal point for the acceleration: optimization based on RSM (Methodology A), optimization based on simulations (Methodology B) and optimization based on combined used of simulations, DOE and RSM (Methodology C). In the optimization based on RSM, the algorithm reaches the optimum point after 600 experiments and a computational cost of six seconds. The results of this optimization are shown in the 2nd column of Table 6. The optimization of the acceleration based on simulations and the relative optimal point was reached with 64 simulations that needed 1 hour of computational cost (the results are listed in the 3rd column of Table 6). In the further optimization (Methodology C in Figure 1), the DE algorithm applied to the response surfaces needed 900 experiments and seven seconds of computational cost to reach the optimum point (the results are listed in the 4th column of Table 6). This optimal configuration is faster to obtained and improved with respect to the previous optimization (3rd column of Table 6) since the acceleration optimum value is of 0.56% lower in comparison to the previous value. It is worth noting that apparently the optimization based on RSM gives the lowest value of acceleration (4.731 m/s$^2$ with respect to 5.845 or 5.812 m/s$^2$ obtained with the other methodologies, see Table 6). However, a simulation performed by using the combination of input variables listed in the 2nd column of Table 6 gives 5.876 m/s$^2$ as acceleration level and not 4.731 m/s$^2$. This contradiction can be explained considering that the acceleration value of 4.731 m/s$^2$ is calculated by using response surfaces with not sufficient predictive capability. In effect the maximum difference between DOE points and RSM points is about 10% that was not satisfactory to guarantee the real physics of the system to be captured by the RSM. On the other hand, the optimal point obtained with Methodology C (5.812 m/s$^2$) coincides with the acceleration level obtained with a simulation performed by using the combination of input variables listed in the 4th column of Table 6. This guarantees the effectiveness and accuracy of Methodology C.

*d. Robust design analysis*

The uncertainty in two input variables (relief groove dimension and radial clearance in the journal bearing) due to the manufacturing tolerances is taken into account. To assess the effect of the input variability for the system response, a probabilistic characterization of the input variables at the optimal configuration has been used. For both the input variables, a normal distribution around the optimum value is considered. Concerning the relief groove dimension, a tolerance of ±0.05 mm and a standard deviation of 0.018 mm are accounted. On the other hand, a tolerance of ±0.0005 mm and a standard deviation of 0.00018 mm are considered for the radial clearance in the journal bearing. Such values can be considered reliable manufactured values. The same analysis of Section 2.4, with Monte Carlo method [26][27] combined with the Latin-Hypercube sampling, has been used to determine the robustness of the optimal configuration. 600 samples are taken for the Monte Carlo analysis. The outcome of the Monte Carlo analysis is an histogram that represents the probabilistic distribution of the system response. Figure 21 presents the distribution of the experiments performed during the Monte Carlo analysis taken as optimum parameter the acceleration. The red bar in the figure represents the optimum point. A standard deviation of 1.08% of the optimal value is obtained. The acceleration exhibits a clear exponential like behavior. As a consequence, small variations in the input parameters used for the robustness assessment may most probably yield small variations of the system responses towards higher accelerations (Figure 21). This

exponential like behavior could be explained considering the response surface depicted in Figure 22. It represents the response surface concerning acceleration, relief groove dimension and radial clearance obtained in step 2C of Figure 1. It is clear that a variation (both towards positive and negative values) of the input variables determines an increase of the acceleration, being the optimal point a minimum of the response surface. Finally, it is worth noting that the above standard deviation values are very low; this means that the input variability due to the manufacturing tolerances does not influence the optimum point. For this reason it is possible to state that the optimal configuration is robust.

## 5. Concluding remarks

This work concerns the development of a methodology (Methodology C) for fast robust design optimization of mechanical systems. In this research activity Methodology C has been applied to two different case studies in order to assess its effectiveness with comparison with standard optimization methodologies (Methodology A and B). Pros and cons of each methodology are underlined and discussed. The new optimization methodology presented in this paper is based on the combined use of simulations, DOE, RSM and DE algorithm. Furthermore, the robustness of the optimal design configuration is also foreseen. The first case study regards a vane pump while the second regards a gear pump for automotive steering applications.
The following concluding remarks can be drawn:

- The new optimization methodology that combines DOE, RSM and evolutionary algorithm (Methodology C) make it possible to reach the optimal configurations faster with respect to the classical optimization based on simulations. Therefore, the combination of DOE, RSM and evolutionary algorithm is an efficient tool in order to refine optimal solutions based on simulations.
- The proposed optimization methodology combined with the parallel computing allows to optimize and to study also complex systems (that are computationally expensive) in a reasonable computational time.
- The use of *ad hoc* RSM obtained by selecting, among a potential functional basis, the functional that mainly influences the overall response, can be considered an effective tool in order to improve the approximation capability of the RSM.
- The proposed methodology allows to reach the optimal configurations and to give response surfaces of good quality that can be used by the designer for further evaluations about dynamical behavior.
- Concerning the vane pump, the optimization methodology has allowed to reach two optimal configurations, one that maximizes the mean output flow rate and one that minimizes the acceleration on the pump casing.
- Concerning the gear pump, the optimization methodology has allowed to determine the configuration that give the lowest acceleration value. Furthermore it was possible to establish that the oil temperature and consequently the Bulk modulus and the oil viscosity strongly influence the casing vibration level. The lower the temperature is, the lower the casing acceleration becomes.
- The uncertainty analysis has established that the detected optimal input configurations are robust, as they are slightly influenced by manufacturing tolerances or small variations in some input parameters.

## 6. Acknowledgements

This work has been developed within the Advanced Mechanics Laboratory (MechLav) of Ferrara Technopole, realized through the contribution of Regione Emilia-Romagna – Assessorato Attività Produttive, Sviluppo Economico, Piano telematico –*POR-FESR* 2007-2013, Activity I.1.1.

## 7. Appendix A

In this Appendix the main geometrical and operational parameters of the vane pump and gear pump being studied are listed.

| Vane pump | | |
|---|---|---|
| **Symbol** | **Value** | **Description** |
| $B_{oil}$ | *1700 MPa* | Oil Bulk modulus |
| $\mu$ | *14 mPa s* | Lubricant dynamic viscosity |
| $\rho$ | *854 kg/m3* | Lubricant density in std conditions |
| $N$ | *11* | Number of vanes |
| $W_S$ | *20 mm* | Pressure ring width |
| $r_S$ | *30 mm* | Pressure ring inner radius |
| $r_r$ | *25 mm* | Rotor shaft radius |
| $t_{vb}$ | *2.2 mm* | Vane thickness at the base |
| $t_{vh}$ | *0.3 mm* | Vane thickness at the head |
| $v_m$ | *0.003 kg* | Vane mass |

| Gear pump | | |
|---|---|---|
| **Value for gear 1** | **Value for gear 2** | **Description** |
| $a$ = 14.65 mm | | Centre distance of gear pair |
| $b_1$ = 12.1 mm | $b_2 = b_1$ | Gear face width |
| $E = 210 \cdot 10^9$ Pa | | Young's modulus |
| $v$ = 0.3 | | Poisson's ratio |
| $J_1 = 4.0714 \cdot 10^{-7}$ kg·m$^2$ | $J_2 = 3.9564 \cdot 10^{-7}$ kg·m$^2$ | Moment of inertia |
| $K_T = 8.053 \cdot 10^2$ Nm/rad | - | Torsional stiffness of the driving shaft |
| $m_1$ = 0.0333 kg | $m_2$ = 0.0216 kg | Mass |
| $\hat{m}$ = 1.150 mm | | Gear module |
| $r_{b1}$ = 6.484 mm | $r_{b2} = r_{b1}$ | Base radius |
| $\hat{x}_1$ = *** | $\hat{x}_2 = \hat{x}_1$ | Addendum modification coefficient (******* confidential) |
| $z_1$ = 12 | $z_2 = z_1$ | Number of teeth |

| | |
|---|---|
| $\alpha$ = 20 deg | Pressure angle |
| $\alpha_w$ = 27.727 deg | Pressure angle in working condition |
| $B_{oil}$ =1400 MPa | Oil Bulk modulus |
| $\mu$=14 mPa s | Lubricant dynamic viscosity |

## 8. References


[1] E. Mucchi, G. Tosi, R. D'Ippolito, G. Dalpiaz, "A robust design optimization methodology for external gear pumps", Proceedings of the ASME 2010 10thBiennal Conference on Engineering Systems Design and Analysis ESDA2010, Istanbul, Turkey, 2010, July 12-14

[2] E Mucchi, G. Dalpiaz, Analysis of the evolution of pressure forces in variable displacement vane pumps using different approaches, Proceedings of the ASME 2013 International Design Engineering Technical Conferences & Computers and Information in Engineering Conference IDETC/CIE 2013 August 4-7, 2013, Portland, Oregon, USA

[3] E. Mucchi, G. Dalpiaz, A. Fernàndez del Rincòn, "Elasto-dynamic analysis of a gear pump. Part I: pressure distribution and gear eccentricity", Mechanical Systems and Signal Processing, 24 (2010), pp. 2160-2179

[4] E. Mucchi, G. Dalpiaz, A. Rivola, "Elasto-dynamic analysis of a gear pump. Part II: meshing phenomena and simulation results", Mechanical System and Signal Processing, 24 (2010) 2180-2197

[5] P. Papalambros, S. Gunawan, K.-Y. Chan, M. Brudnak, G. Van den Bergh, "Software Integration for Simulation-Based Analysis and Robust Design Automation of HMMWV Rollover Bahavior", 2007 SAE International

[6] C. Zang, M.I. Friswell, J.E. Mottershead, "A review of robust optimal design and its application in dynamics", Computers and Structures 83 (2005) 315-326

[7] R.V.Rao, V.J. Savsani, D.P. Vakharia, "Teaching-learning-based optimization: A novel method for constrained mechanical design optimization problems", Computer-Aided Design 43 (2011) 303-315

[8] J.A. Snyman, A.M. Hay, "The Dynamic-Q Optimization Method: An Alternative to SPQ?", Computers and Mathematics with Applications 44 (2002) 1589-1598

[9] G. Steenackers, F. Presezniak, P. Guillaume, "Development of an adaptive response surface method for optimization of computation-intensive models", Computers & Industrial Engineering 57 (2009) 847-855

[10] P. Breitkopf, H. Naceur, A. Rassineux, P. Villon, "Moving least squares response surface approximation: Formulation and metal forming applications", Computers and Structures 83 (2005) 1411-1428.

[11] CHEN Wei, ZHOU Xiong-hui, WANG Hui-feng, WANG Wan, "Multi-Objective Optimal Approach for Injection Molding Based on Surrogate Model and Particle Swarm Optimization Algorithm", J. Shanghai Jiaotong Univ. (Sci.), 2010, 15(1): 88-93.

[12] Carlos A. Henao and Christos T. Maravelias, Surrogate-Based Superstructure Optimization Framework, AIChE Journal, May 2011 Vol. 57, No. 5.

[13] R. Rikards, H. Abramovich, J. Auzins, A. Korjakins, O. Ozolinsh, K. Kalnins, T. Green Surrogate models for optimum design of stiffened composite shells, Composite Structures 63 (2004) 243–251.

[14] Nestor V. Queipo, Carlos J. Arevalo, Salvador Pintos, The integration of design of experiments, surrogate modeling and optimization for thermoscience research, Engineering with Computers (2005) 20: 309–315.

[15] V.M. Perez, J.E. Renaud and L.T. Watson, Adaptive experimental design for construction of response surface approximation, AIAA J 40 (12) (2002, pp. 2495-2503)

[16] Thomas J. Lorenzen, Virgil L. Anderson, "Design of Experiments, A No-Name Approach", Marcel Dekker, Inc, 1993

[17] T. Krishnamurthy, "Response Surface Approximation with Augmented and Compactly Supported Radial Basis Functions", Proceedings of 44th AIAA/ASME/ASCE/AHS/ASC, Norfolk, Virginia, 7-10 April 2003

[18] R. Storn and K. Price, "Minimizing the real function of ICEC'96 contest by Differential Evolutions", Proceedings of the international Conference on Evolutionary Computation, Nagoya, Japan, 1996

[19] Panos Y. Papalambros and Douglas J. Wilde, "Principles of Optimal Design", Cambridge University Press

[20] Noesis Solutions, OPTIMUS Theoretical Background, November 2008, Leuven, Belgium

[21] Barbarelli S., Bova S. and Piccione R., 2009, "Zero-dimensional model and pressure data analysis of a variable-displacement lubricating vane pump", SAE International (2009-01-1859)

[22] Cantore G., Paltrinieri F., Tosetti F. and Milani M., 2008, "Lumped parameters numerical simulation of a variable displacement vane pump for high speed ice lubrification", SAE International (2008-01-2445)

[23] E. Mucchi, G.Dalpiaz, A. Rivola, "Dynamic behaviour of gear pumps: effect of variations in operational and design parameters", Meccanica Volume 46, Issue 6 (2011), 1191-1212

[24] S.M. Sanchez, "A Robust Design Tutorial", Proceedings of the 1994 Winter Simulation Conference ed. J.D. Tew, S. Manivannan, D.A. Sadowski and A.F. Seila

[25] G. Taguchi, Quality engineering (Taguchi Methods) for the development of electronic circuit technology, IEEE Transactions on Reliability, 44(2), pp. 225-229 (June 1995)

[26] Kalos MH, Whitlock PA, "Monte Carlo methods: vol. 1st, basics", New York, Wiley, 1986

[27] Schinozuka M., "Monte Carlo solution of structural dynamics", Computers and Structures 2 (1972) 855-874

[28] D'Ippolito R., Donders S., Van der Auweraer H., "Virtual Prototypes for Uncertainty and Variability-Based Product Engineering", in Product Engineering:Tools and Methods based on Virtual Reality, p.427-448, Editors D. Talabă and A. Amditis, Springer, Dordrecht, The Netherlands, 2008

[29] E. Mucchi, G. D'Elia, G. Dalpiaz, "Simulation of the running in process in external gear pumps and experimental verification", Meccanica Volume 47, Issue 3 (2012), 621-637

[30] E. Mucchi, A. Rivola, G. Dalpiaz, Modelling dynamic behaviour and noise generation in gear pumps: Procedure and validation, Applied Acoustics 77 (2014) 99-111.

[31] Zardin B., Paltrinieri F., Brghi M., Milani M., “About the prediction of pressure variation in the inter-teeth volumes of external gear pumps”, Proceedings of the 3rd FPNI-PhD Symposium on Fluid Power, 2004 Terrassa, Spain, June 30 - July 2

[32] Borghi M., Bonacini C., “Calcolo delle pressioni sui fianchi degli ingranaggi di machine oleodinamiche ad ingranaggi esterni”, Oleodinamica-Pneumatica, 118-124, Aprile 1991

[33] Childs D., Moes H., Van Leeuwen H., “Journal bearing impedance descriptions for rotordynamic application”, Journal of Lubrication Technoogy 99 (1997), 198-214.

# FIGURES

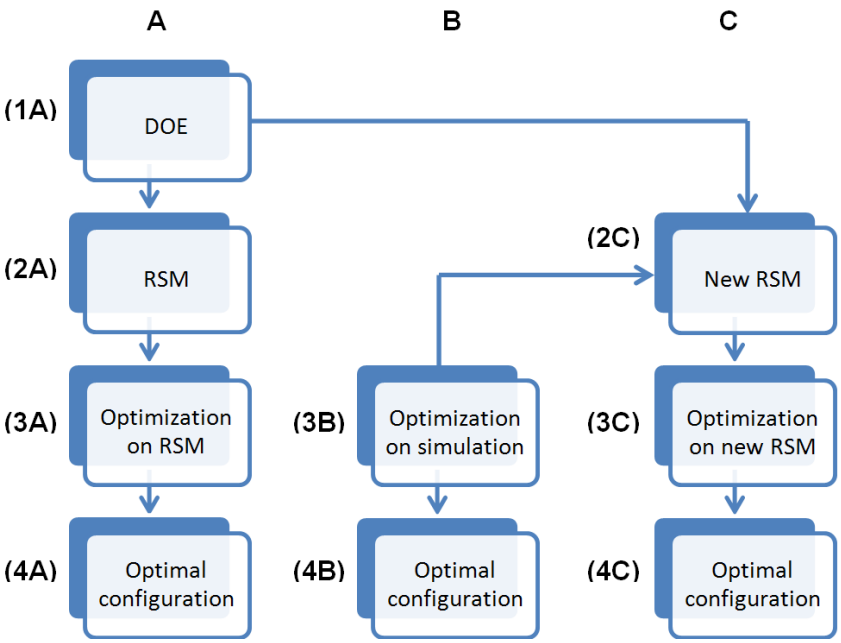


**Figure 1 – Schematic of the optimization methodologies**

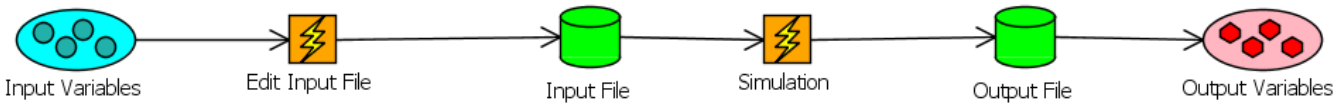


**Figure 2 – OPTIMUS workflow**

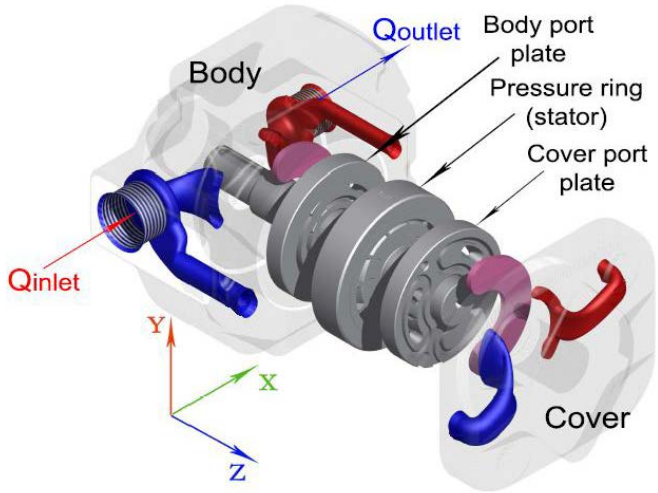


**Figure 3 - Exploded view of vane pump with distribution ducts**

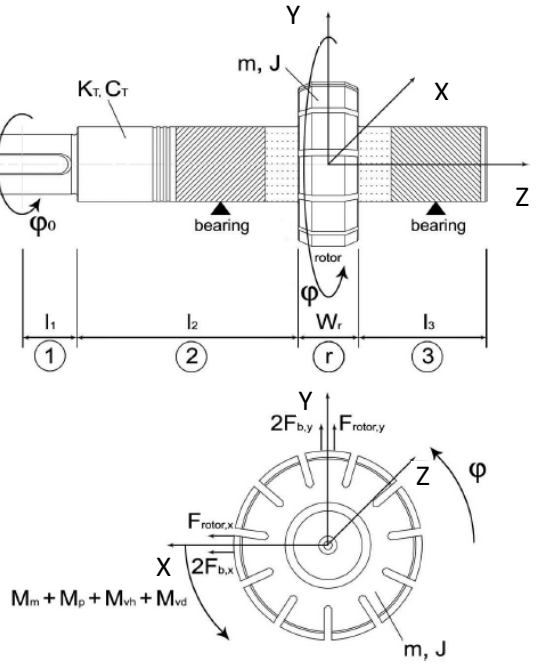


**Figure 4 – Lumped Parameter model of the vane pump rotor shaft**

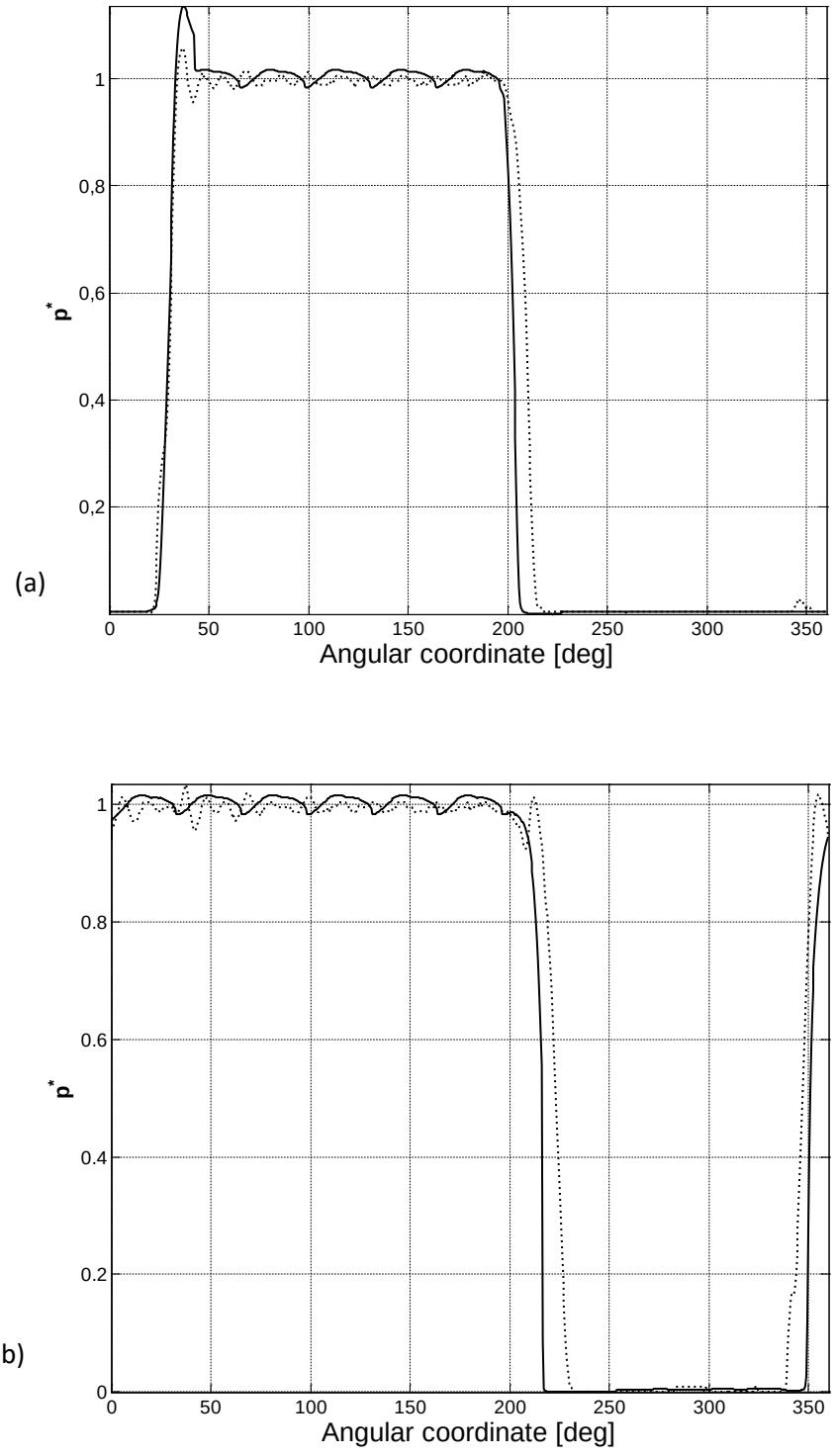


**Figure 5 - Normalized pressure evolution for a complete shaft rotation in a vane space (a) and in a hole (b) referred to pump PHV 05: experimental (dash-dot line) and LP model results (solid line). Full flow condition.**

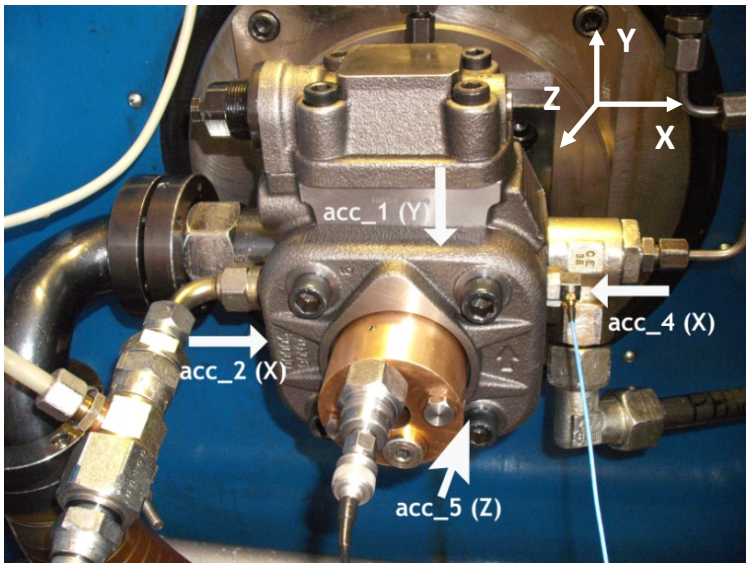


**Figure 6 – Photo of the vane pump**

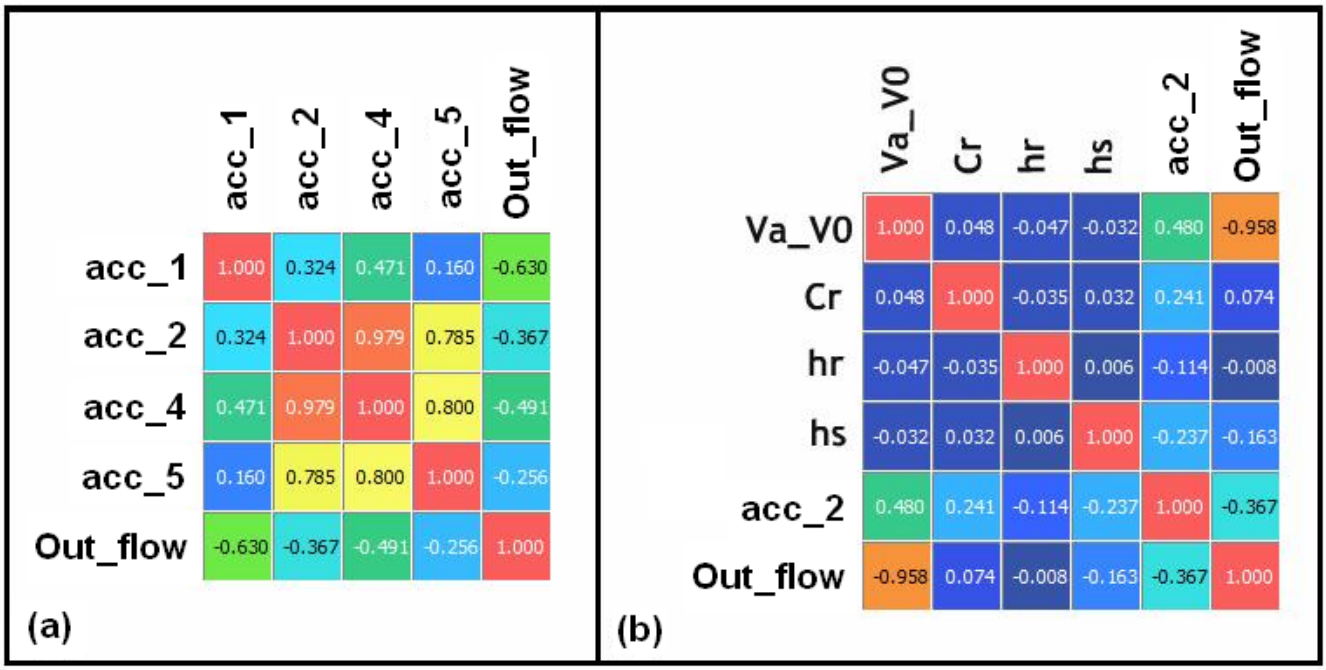


**Figure 7 – Correlation matrices between output variables (a) and between input and output variables (b) for DOE (vane pump)**

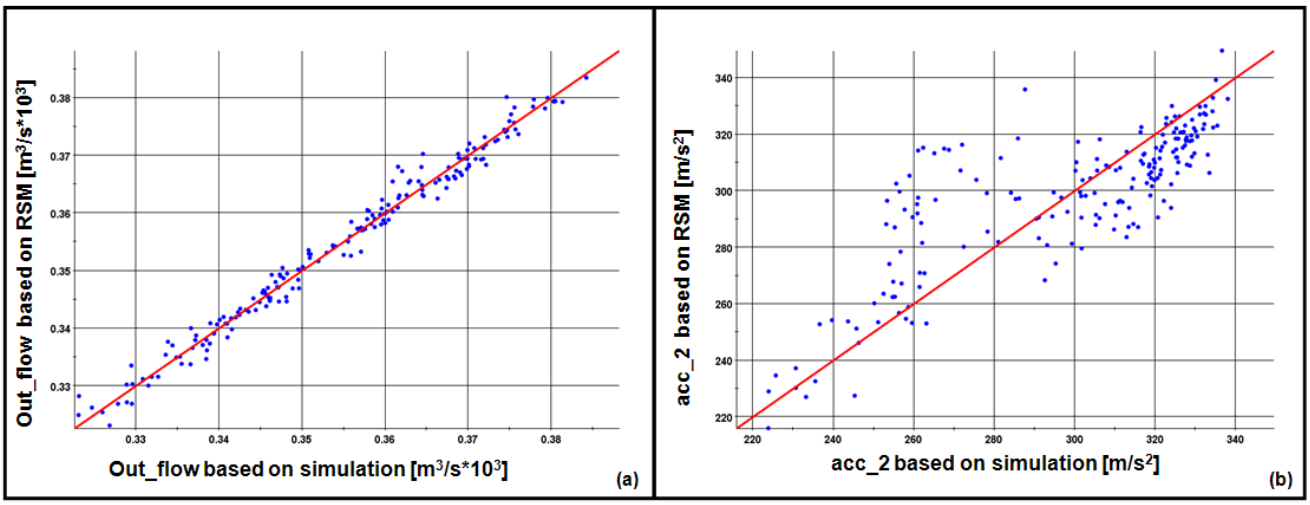


**Figure 8 – Comparison between RSM (Taylor Polynomials) and simulation results for the output flow (a) and for the acceleration (b)**

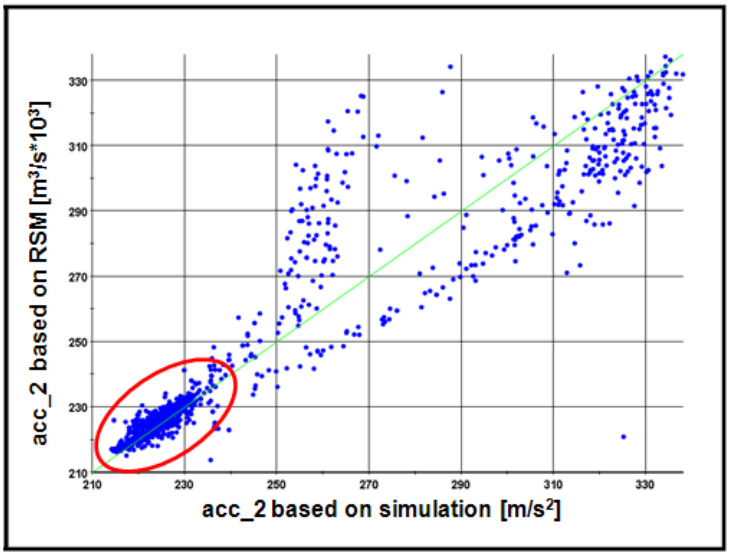


**Figure 9 - Comparison between new RSM (Taylor Polynomials) and simulation results for the acceleration**

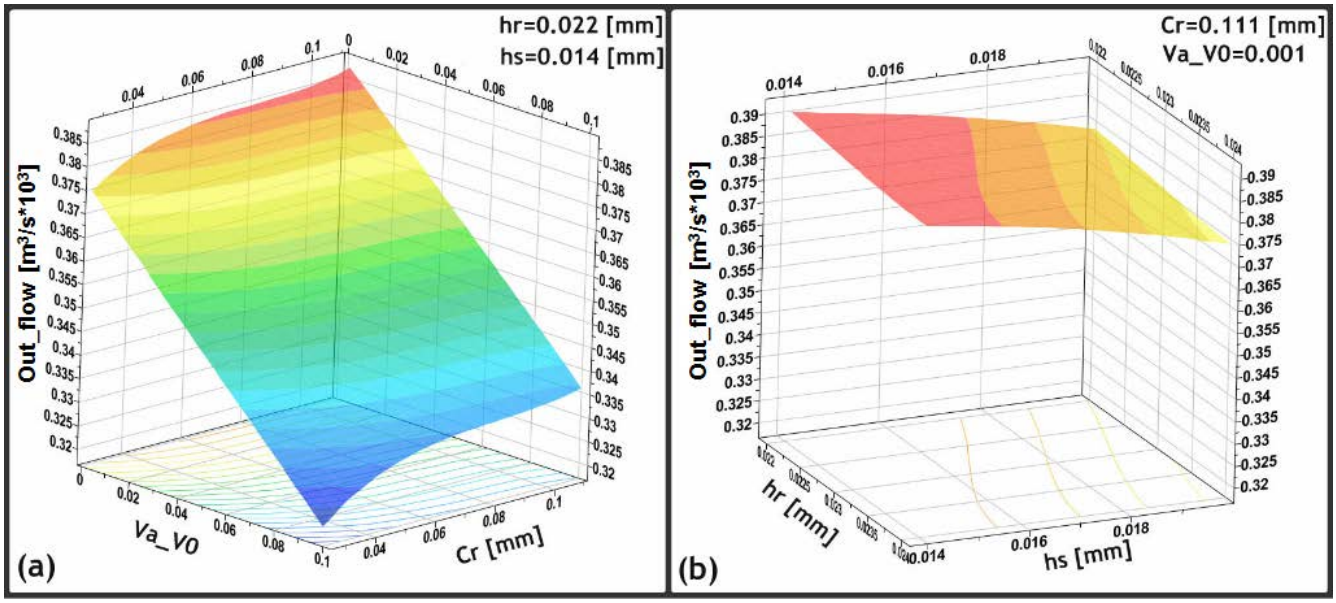


**Figure 10 – Response surfaces obtained in step 2C concerning (a) mean output flow, ratio between air and oil volume, radial clearance, (b) mean output flow, clearance between rotor and port plates, clearance between ring and port plates**

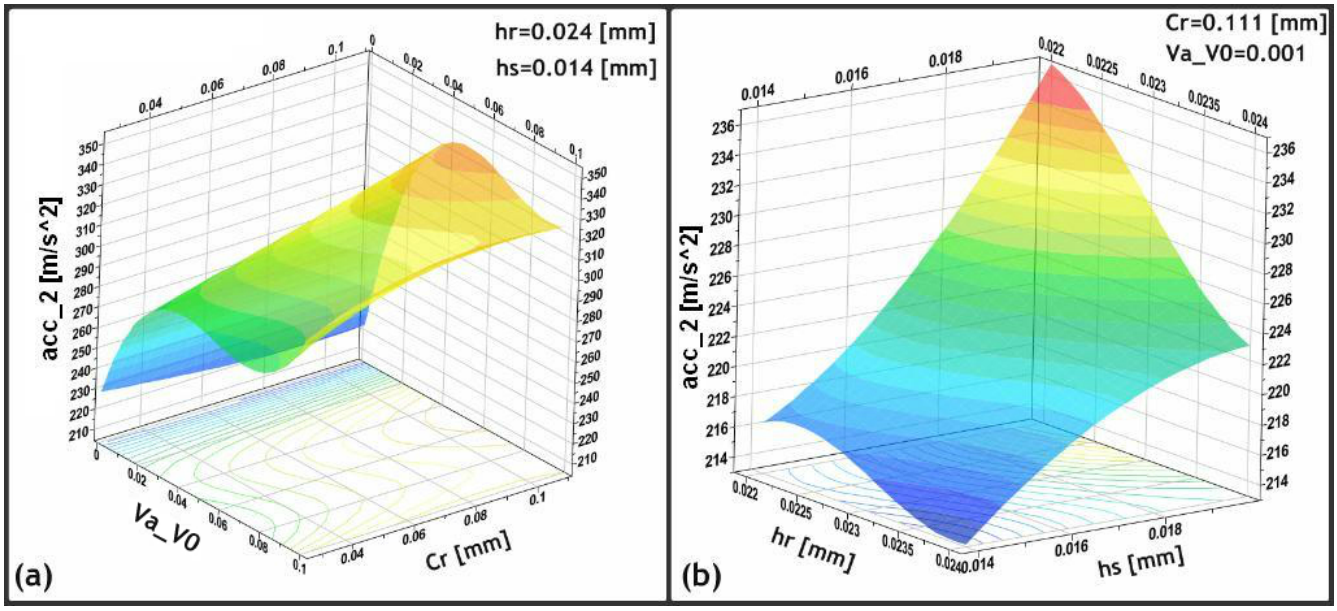


**Figure 11 - Response surfaces obtained in step 2C concerning (a) acceleration, ratio between air and oil volume, radial clearance, (b) acceleration, clearance between rotor and port plates, clearance between ring and port plates**

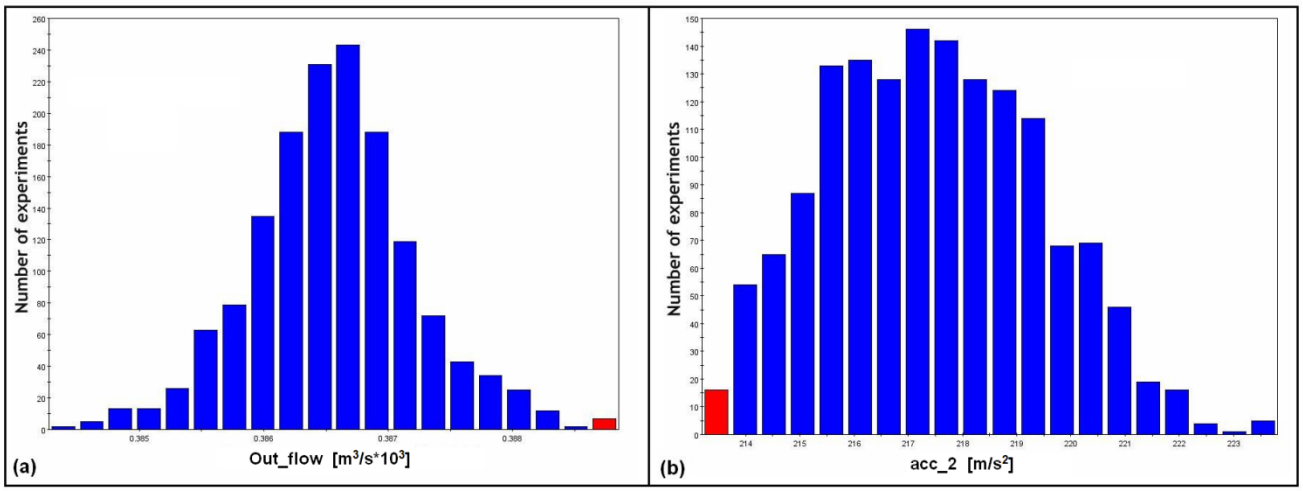


**Figure 12 – Output distribution related to the robust design analysis on (a) mean volumetric flow rate optimization, (b) acceleration optimization**

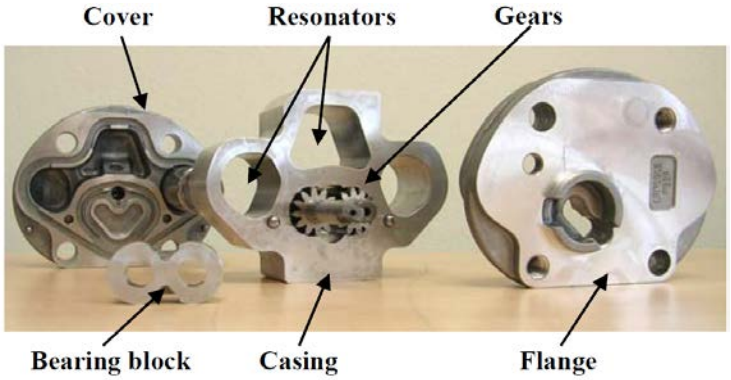


**Figure 13 – Photo of the gear pump**

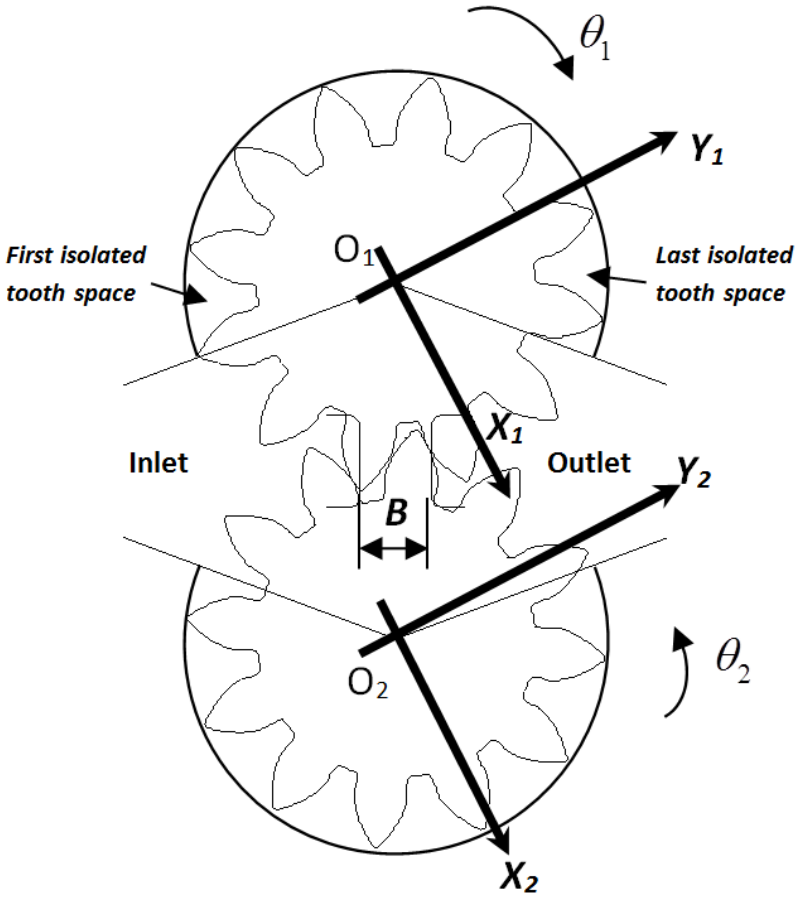


**Figure 14 – Schematic of the gear pump and reference frames.**

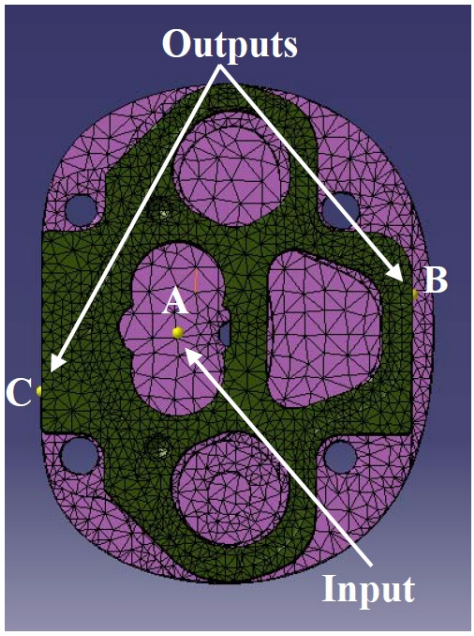


**Figure 15 – Input and output points set in the FRF analysis**

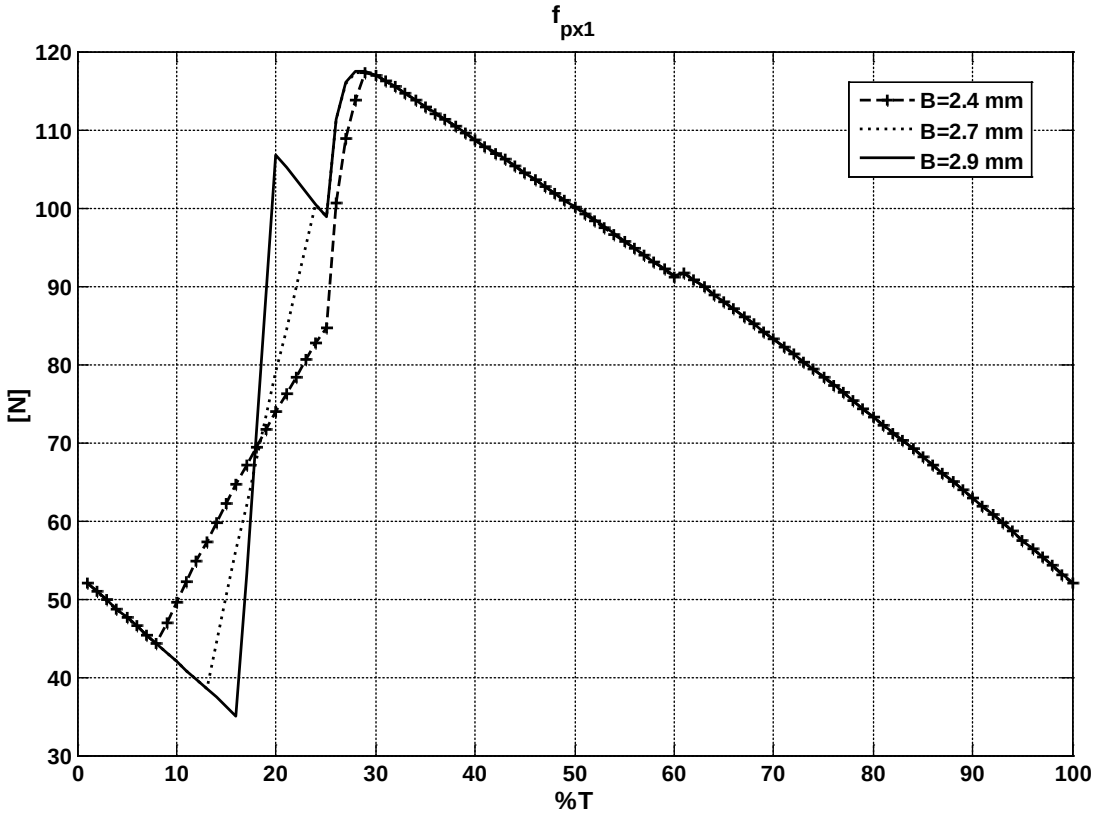


**Figure 16– Pressure force on gear 1 in direction $X_1$ over one meshing period T with different relief groove dimensions (B)**

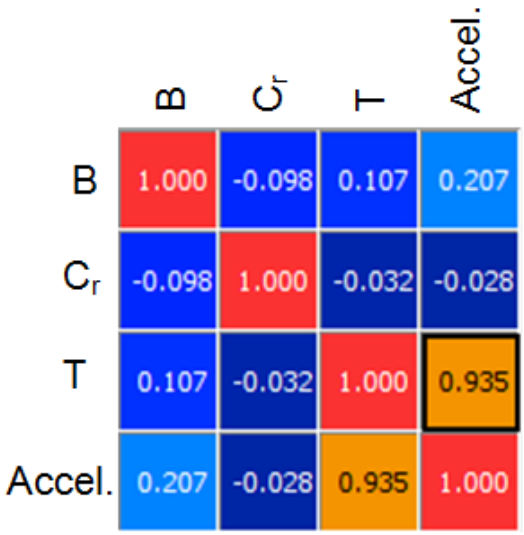


**Figure 17 – Correlation matrix between input and output variables for DOE (gear pump)**

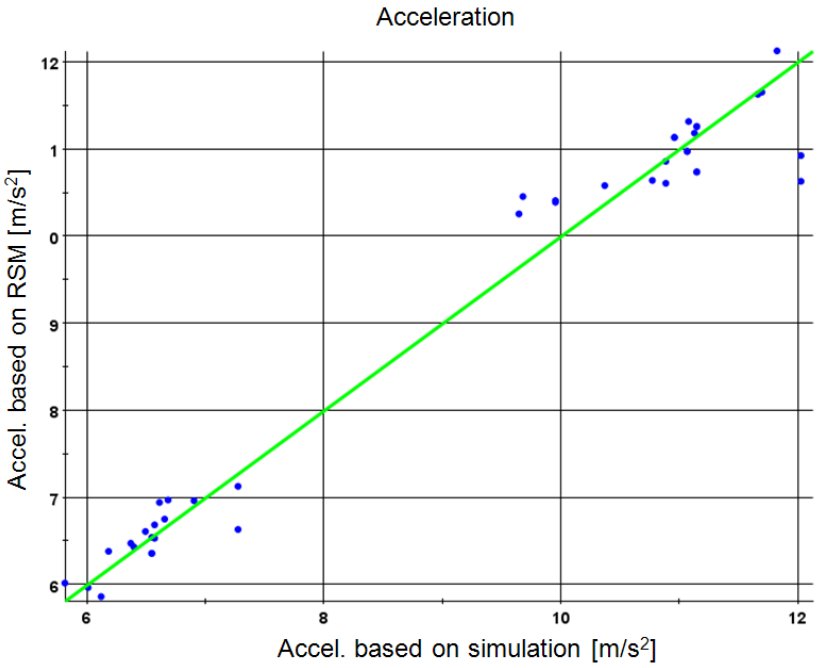


**Figure 18 – Comparison between RSM (Taylor Polynomials) and simulation results for the acceleration**

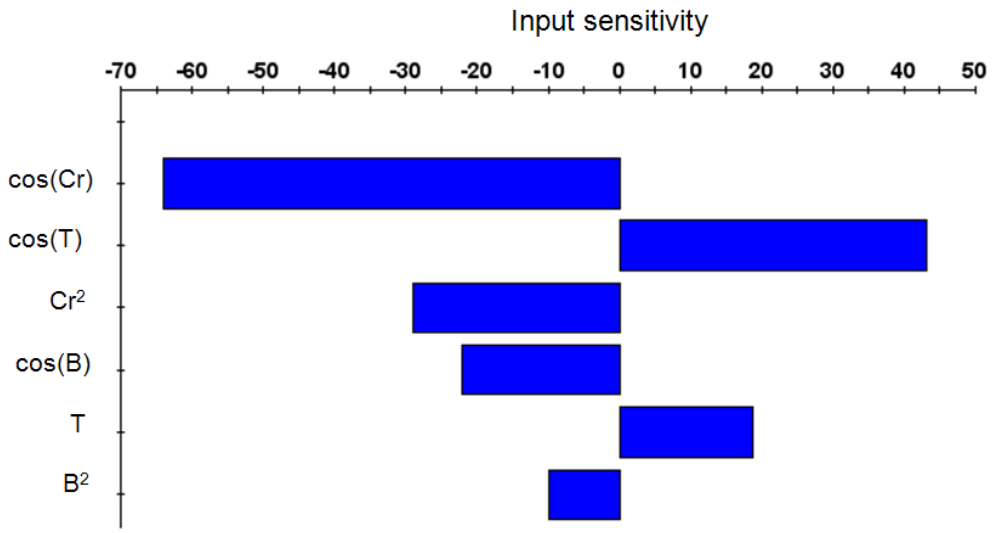


**Figure 19 – Contribution plot for the acceleration based on RSM (functional coefficients)**

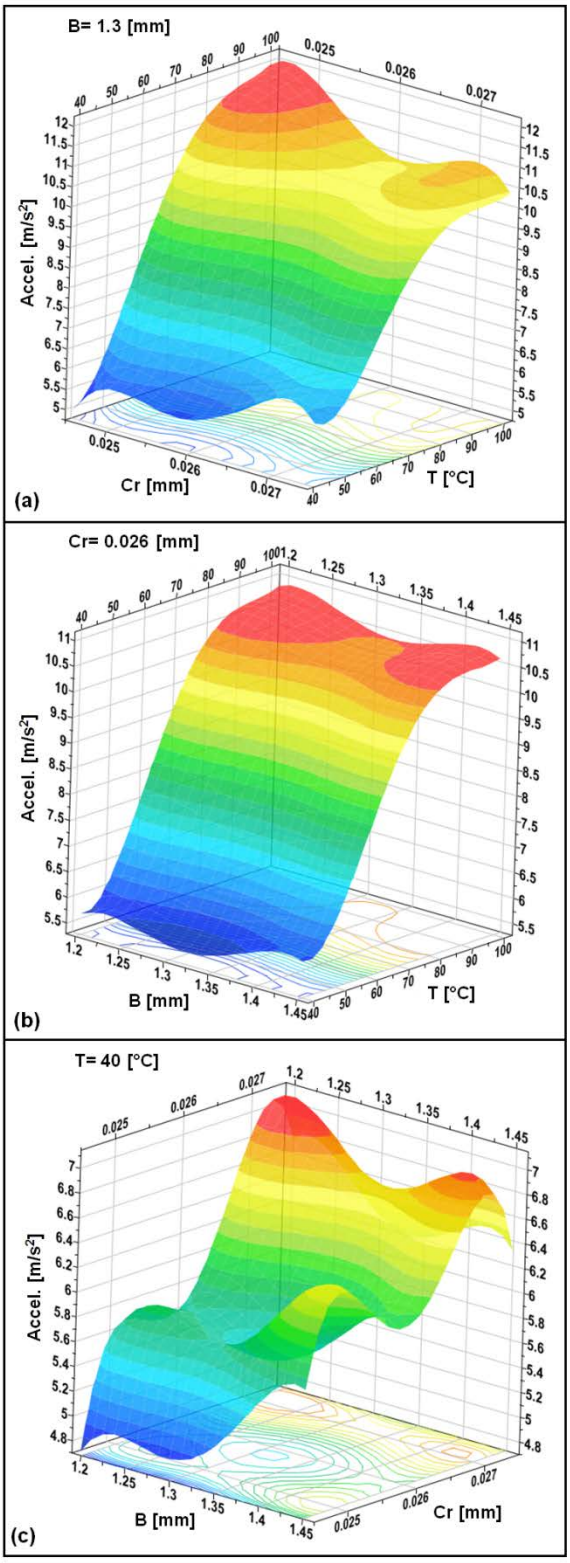


**Figure 20 – Response surfaces obtained in step 2A concerning (a) acceleration, radial clearance and oil temperature, (b) acceleration, relief groove dimension and oil temperature, (c) acceleration, relief groove dimension and radial clearance**

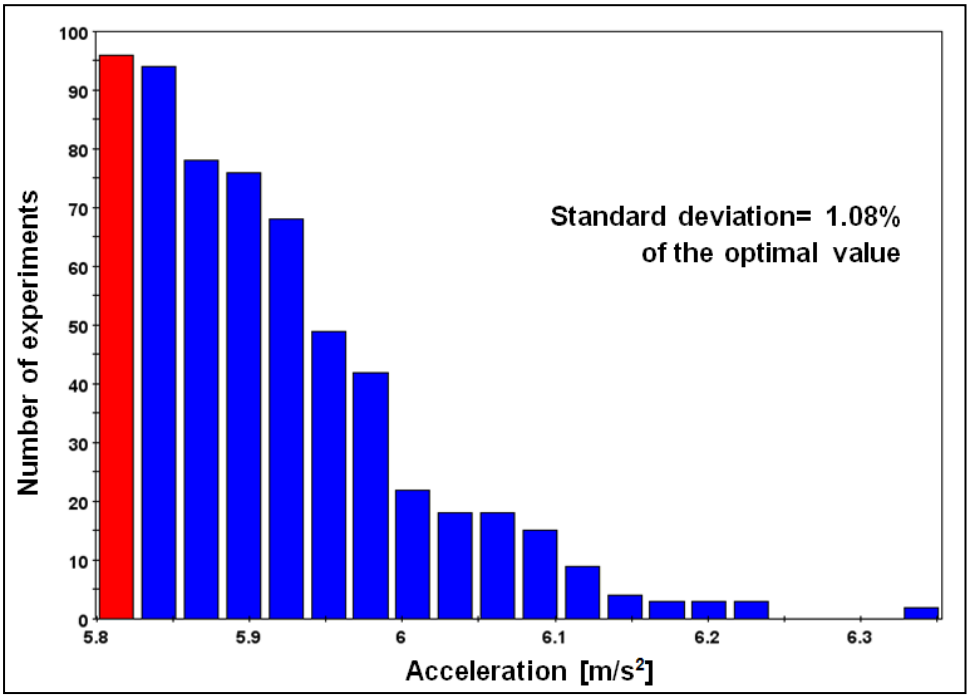


**Figure 21 – Output distribution related to the robust design analysis on the acceleration optimization**

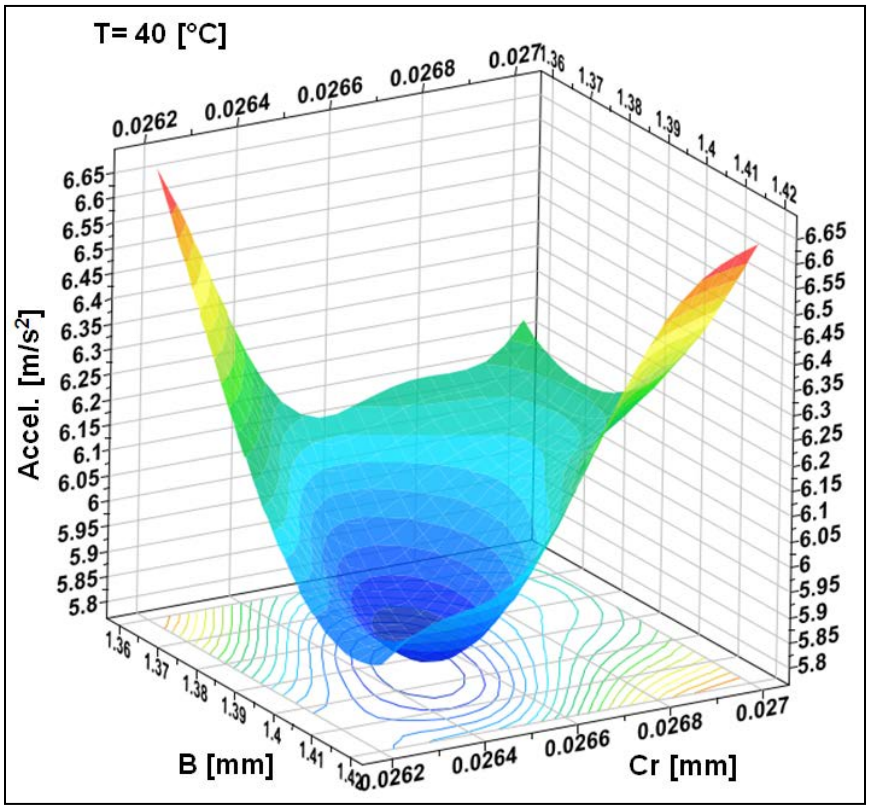


**Figure 22 – Response surface obtained in step 2C concerning acceleration, relief groove dimension and radial clearance around the optimal acceleration point of step 4C**

# TABLES

| Input variables | Symbols | Variability | | | |
|---|---|---|---|---|---|
| | | Nominal value | Low boundary | High boundary | Step |
| Ratio between air volume and oil volume | Va_Vo | 0.005 | 0.001 | 0.1 | 0.001 |
| Radial clearance in the journal bearing [mm] | Cr | 0.063 | 0.025 | 0.111 | 0.001 |
| Thickness of the meatus between rotor and port plates [mm] | hr | 0.023 | 0.022 | 0.024 | 0.0005 |
| Thickness of the meatus between pressure ring and port plates [mm] | hs | 0.015 | 0.014 | 0.02 | 0.0005 |

**Table 1 – Input variable definition and relative variability ranges for the vane pump**

| Input | Optimization of the flow rate Methodology A | Optimization of the flow rate Methodology C |
|---|---|---|
| Va_V0 | 0.001 | 0.001 |
| Cr [mm] | 0.111 | 0.111 |
| hr [mm] | 0.022 | 0.022 |
| hs [mm] | 0.014 | 0.014 |
| Out_flow [$m^3/s*10^3$] | 0.39308 | 0.3911 |

**Table 2 – Mean output flow rate optimization results**

| Input | Optimization of the acceleration Methodology A | Optimization of the acceleration Methodology B | Optimization of the acceleration Methodology C |
|---|---|---|---|
| Va_V0 | 0.001 | 0.002 | 0.001 |
| Cr [mm] | 0.025 | 0.065 | 0.111 |
| hr [mm] | 0.024 | 0.0235 | 0.024 |
| hs [mm] | 0.014 | 0.0155 | 0.014 |
| acc_2 [m/s$^2$] | 144.06 | 214.72 | 213.13 |

**Table 3 – Acceleration optimization results**

| Input variable | Tolerance | Standard deviation |
|---|---|---|
| Cr | -0.003 | 0.001 |
| hr | -0.0015 | 0.0005 |
| hs | +0.0014 | 0.0005 |
| Va_Vo | +0.001 | 0.001 |

**Table 4 – Tolerances and standard deviations considered in the robust design analysis**

| Input variable | Symbol | Variability | | | |
|---|---|---|---|---|---|
| *Constant values* | | *Value* | | | |
| Output pressure [bar] | $p_{out}$ | 70 | | | |
| Rotational speed [rpm] | $\omega$ | 1660 | | | |
| *Stepped values* | | *Nominal value* | *Low boundary* | *High boundary* | *Step* |
| Relief groove dimension [mm] | $B$ | 1.45 | 1.2 | 1.45 | 0.05 |
| Radial clearance in the journal bearing [mm] | $Cr$ | 0.0245 | 0.0245 | 0.0275 | 0.0005 |
| *List of values* | | *List of values* | | | |
| Temperature [°C] | $T$ | 40 | 50 | 80 | 100 |
| Bulk modulus [bar] | $B_{oil}$ | 7415 | 7856 | 9178 | 10418 |
| Dynamic viscosity [mPa*s] | $\mu$ | 16.26 | 14.08 | 7.547 | 6.15 |

**Table 5 – Input variable definition and relative variability ranges**

| Input | Optimization of the acceleration<br>Methodology A | Optimization of the acceleration<br>Methodology B | Optimization of the acceleration<br>Methodology C |
|---|---|---|---|
| B [mm] | 1.2 | 1.4 | 1.4 |
| Cr [mm] | 0.0245 | 0.025 | 0.0265 |
| T [°C] | 40 | 40 | 40 |
| $B_{oil}$ [bar] | 7415 | 7415 | 7415 |
| μ [mPa*s] | 16.26 | 16.26 | 16.26 |
| Accel. [m/s$^2$] | 4.731 | 5.845 | 5.812 |

**Table 6 – Acceleration optimization results**